Jet pseudorapidity distribution in direct photon events in $p\bar{p}$ collisions at $\sqrt{s}=1.8$ TeV

F. Abe,[13] M. G. Albrow,[7] S. R. Amendolia,[22] D. Amidei,[16] J. Antos,[28] C. Anway-Wiese,[4] G. Apollinari,[26] H. Areti,[7] M. Atac,[7] P. Auchincloss,[25] F. Azfar,[21] P. Azzi,[20] N. Bacchetta,[20] W. Badgett,[16] M. W. Bailey,[18] J. Bao,[35] P. de Barbaro,[25] A. Barbaro-Galtieri,[14] V. E. Barnes,[24] B. A. Barnett,[12] P. Bartalini,[22] G. Bauer,[15] T. Baumann,[9] F. Bedeschi,[22] S. Behrends,[3] S. Belforte,[22] G. Bellettini,[22] J. Bellinger,[34] D. Benjamin,[31] J. Benlloch,[15] J. Bensinger,[3] D. Benton,[21] A. Beretvas,[7] J. P. Berge,[7] S. Bertolucci,[8] A. Bhatti,[26] K. Biery,[11] M. Binkley,[7] F. Bird,[29] D. Bisello,[20] R. E. Blair,[1] C. Blocker,[3] A. Bodek,[25] W. Bokhari,[15] V. Bolognesi,[22] D. Bortoletto,[24] C. Boswell,[12] T. Boulos,[14] G. Brandenburg,[9] C. Bromberg,[17] E. Buckley-Geer,[7] H. S. Budd,[25] K. Burkett,[16] G. Busetto,[20] A. Byon-Wagner,[7] K. L. Byrum,[1] J. Cammerata,[12] C. Campagnari,[7] M. Campbell,[16] A. Caner,[7] W. Carithers,[14] D. Carlsmith,[34] A. Castro,[20] Y. Cen,[21] F. Cervelli,[22] H. Y. Chao,[28] J. Chapman,[16] M.-T. Cheng,[28] G. Chiarelli,[22] T. Chikamatsu,[32] C. N. Chiou,[28] L. Christofek,[10] S. Cihangir,[7] A. G. Clark,[22] M. Cobal,[22] M. Contreras,[5] J. Conway,[27] J. Cooper,[7] M. Cordelli,[8] C. Couyoumtzelis,[22] D. Crane,[1] J. D. Cunningham,[3] T. Daniels,[15] F. DeJongh,[7] S. Delchamps,[7] S. Dell'Agnello,[22] M. Dell'Orso,[22] L. Demortier,[26] B. Denby,[22] M. Deninno,[2] P. F. Derwent,[16] T. Devlin,[27] M. Dickson,[25] J. R. Dittmann,[6] S. Donati,[22] R. B. Drucker,[14] A. Dunn,[16] K. Einsweiler,[14] J. E. Elias,[7] R. Ely,[14] E. Engels, Jr.,[23] S. Eno,[5] D. Errede,[10] S. Errede,[10] Q. Fan,[25] B. Farhat,[15] I. Fiori,[2] B. Flaugher,[7] G. W. Foster,[7] M. Franklin,[9] M. Frautschi,[18] J. Freeman,[7] J. Friedman,[15] H. Frisch,[5] A. Fry,[29] T. A. Fuess,[1] Y. Fukui,[13] S. Funaki,[32] G. Gagliardi,[22] S. Galeotti,[22] M. Gallinaro,[20] A. F. Garfinkel,[24] S. Geer,[7] D. W. Gerdes,[16] P. Giannetti,[22] N. Giokaris,[26] P. Giromini,[8] L. Gladney,[21] D. Glenzinski,[12] M. Gold,[18] J. Gonzalez,[21] A. Gordon,[9] A. T. Goshaw,[6] K. Goulianos,[26] H. Grassmann,[6] A. Grewal,[21] L. Groer,[27] C. Grosso-Pilcher,[5] C. Haber,[14] S. R. Hahn,[7] R. Hamilton,[9] R. Handler,[34] R. M. Hans,[35] K. Hara,[32] B. Harral,[21] R. M. Harris,[7] S. A. Hauger,[6] J. Hauser,[4] C. Hawk,[27] J. Heinrich,[21] D. Cronin-Hennessy,[6] R. Hollebeek,[21] L. Holloway,[10] A. Hölscher,[11] S. Hong,[16] G. Houk,[21] P. Hu,[23] B. T. Huffman,[23] R. Hughes,[25] P. Hurst,[9] J. Huston,[17] J. Huth,[9] J. Hylen,[7] M. Incagli,[22] J. Incandela,[7] H. Iso,[32] H. Jensen,[7] C. P. Jessop,[9] U. Joshi,[7] R. W. Kadel,[14] E. Kajfasz,[7,*] T. Kamon,[30] T. Kaneko,[32] D. A. Kardelis,[10] H. Kasha,[35] Y. Kato,[19] L. Keeble,[8] R. D. Kennedy,[27] R. Kephart,[7] P. Kesten,[14] D. Kestenbaum,[9] R. M. Keup,[10] H. Keutelian,[7] F. Keyvan,[4] D. H. Kim,[7] H. S. Kim,[11] S. B. Kim,[16] S. H. Kim,[32] Y. K. Kim,[14] L. Kirsch,[3] P. Koehn,[25] K. Kondo,[32] J. Konigsberg,[9] S. Kopp,[5] K. Kordas,[11] W. Koska,[7] E. Kovacs,[7,*] W. Kowald,[6] M. Krasberg,[16] J. Kroll,[7] M. Kruse,[24] S. E. Kuhlmann,[1] E. Kuns,[27] A. T. Laasanen,[24] N. Labanca,[22] S. Lammel,[4] J. I. Lamoureux,[3] T. LeCompte,[10] S. Leone,[22] J. D. Lewis,[7] P. Limon,[7] M. Lindgren,[4] T. M. Liss,[10] N. Lockyer,[21] C. Loomis,[27] O. Long,[21] M. Loreti,[20] E. H. Low,[21] J. Lu,[30] D. Lucchesi,[22] C. B. Luchini,[10] P. Lukens,[7] J. Lys,[14] P. Maas,[34] K. Maeshima,[7] A. Maghakian,[26] P. Maksimovic,[15] M. Mangano,[22] J. Mansour,[17] M. Mariotti,[20] J. P. Marriner,[7] A. Martin,[10] J. A. J. Matthews,[18] R. Mattingly,[15] P. McIntyre,[30] P. Melese,[26] A. Menzione,[22] E. Meschi,[22] G. Michail,[9] S. Mikamo,[13] M. Miller,[5] R. Miller,[17] T. Mimashi,[32] S. Miscetti,[8] M. Mishina,[13] H. Mitsushio,[32] S. Miyashita,[32] Y. Morita,[32] S. Moulding,[26] J. Mueller,[27] A. Mukherjee,[7] T. Muller,[4] P. Musgrave,[11] L. F. Nakae,[29] I. Nakano,[32] C. Nelson,[7] D. Neuberger,[4] C. Newman-Holmes,[7] L. Nodulman,[1] S. Ogawa,[32] S. H. Oh,[6] K. E. Ohl,[35] R. Oishi,[32] T. Okusawa,[19] C. Pagliarone,[22] R. Paoletti,[22] V. Papadimitriou,[31] S. P. Pappas,[35] S. Park,[7] J. Patrick,[7] G. Pauletta,[22] M. Paulini,[14] L. Pescara,[20] M. D. Peters,[14] T. J. Phillips,[6] G. Piacentino,[2] M. Pillai,[25] R. Plunkett,[7] L. Pondrom,[34] N. Produit,[14] J. Proudfoot,[1] F. Ptohos,[9] G. Punzi,[22] K. Ragan,[11] F. Rimondi,[2] L. Ristori,[22] M. Roach-Bellino,[33] W. J. Robertson,[6] T. Rodrigo,[7] J. Romano,[5] L. Rosenson,[15] W. K. Sakumoto,[25] D. Saltzberg,[5] A. Sansoni,[8] V. Scarpine,[30] A. Schindler,[14] P. Schlabach,[9] E. E. Schmidt,[7] M. P. Schmidt,[35] O. Schneider,[14] G. F. Sciacca,[22] A. Scribano,[22] S. Segler,[7] S. Seidel,[18] Y. Seiya,[32] G. Sganos,[11] A. Sgolacchia,[2] M. Shapiro,[14] N. M. Shaw,[24] Q. Shen,[24] P. F. Shepard,[23] M. Shimojima,[32] M. Shochet,[5] J. Siegrist,[29] A. Sill,[31] P. Sinervo,[11] P. Singh,[23] J. Skarha,[12] K. Sliwa,[33] D. A. Smith,[22] F. D. Snider,[12] L. Song,[7] T. Song,[16] J. Spalding,[7] L. Spiegel,[7] P. Sphicas,[15] L. Stanco,[20] J. Steele,[34] A. Stefanini,[22] K. Strahl,[11] J. Strait,[7] D. Stuart,[7] G. Sullivan,[5] K. Sumorok,[15] R. L. Swartz, Jr.,[10] T. Takahashi,[19] K. Takikawa,[32] F. Tartarelli,[22] W. Taylor,[11] P. K. Teng,[28] Y. Teramoto,[19] S. Tether,[15] D. Theriot,[7] J. Thomas,[29] T. L. Thomas,[18] R. Thun,[16] M. Timko,[33] P. Tipton,[25] A. Titov,[26] S. Tkaczyk,[7] K. Tollefson,[25] A. Tollestrup,[7] J. Tonnison,[24] J. F. de Troconiz,[9] J. Tseng,[12] M. Turcotte,[29] N. Turini,[22] N. Uemura,[32] F. Ukegawa,[21] G. Unal,[21] S. C. van den Brink,[23] S. Vejcik III,[16] R. Vidal,[7] M. Vondracek,[10] D. Vucinic,[15] R. G. Wagner,[1] R. L. Wagner,[7] N. Wainer,[7] R. C. Walker,[25] C. Wang,[6] C. H. Wang,[28] G. Wang,[22] J. Wang,[5] M. J. Wang,[28] Q. F. Wang,[26] A. Warburton,[11] G. Watts,[25] T. Watts,[27] R. Webb,[30] C. Wei,[6] C. Wendt,[34] H. Wenzel,[14] W. C. Wester III,[7] T. Westhusing,[10] A. B. Wicklund,[1] E. Wicklund,[7] R. Wilkinson,[21] H. H. Williams,[21] P. Wilson,[5] B. L. Winer,[25] J. Wolinski,[30] D. Y. Wu,[16] X. Wu,[22] J. Wyss,[20] A. Yagil,[7] W. Yao,[14] K. Yasuoka,[32] Y. Ye,[11] G. P. Yeh,[7] P. Yeh,[28] M. Yin,[6] J. Yoh,[7] C. Yosef,[17] T. Yoshida,[19] D. Yovanovitch,[7] I. Yu,[35] J. C. Yun,[7] A. Zanetti,[22] F. Zetti,[22] L. Zhang,[34] S. Zhang,[16] W. Zhang,[21] and S. Zucchelli[2]

(CDF Collaboration)

[1]*Argonne National Laboratory, Argonne, Illinois 60439*

[2]*Istituto Nazionale di Fisica Nucleare, University of Bologna, I-40126 Bologna, Italy*

[3]*Brandeis University, Waltham, Massachusetts 02254*

[4]*University of California at Los Angeles, Los Angeles, California 90024*
[5]*University of Chicago, Chicago, Illinois 60637*
[6]*Duke University, Durham, North Carolina 27708*
[7]*Fermi National Accelerator Laboratory, Batavia, Illinois 60510*
[8]*Laboratori Nazionali di Frascati, Istituto Nazionale di Fisica Nucleare, I-00044 Frascati, Italy*
[9]*Harvard University, Cambridge, Massachusetts 02138*
[10]*University of Illinois, Urbana, Illinois 61801*
[11]*Institute of Particle Physics, McGill University, Montreal, Canada H3A 2T8*
and University of Toronto, Toronto, Canada M5S 1A7
[12]*The Johns Hopkins University, Baltimore, Maryland 21218*
[13]*National Laboratory for High Energy Physics (KEK), Tsukuba, Ibaraki 305, Japan*
[14]*Lawrence Berkeley Laboratory, Berkeley, California 94720*
[15]*Massachusetts Institute of Technology, Cambridge, Massachusetts 02139*
[16]*University of Michigan, Ann Arbor, Michigan 48109*
[17]*Michigan State University, East Lansing, Michigan 48824*
[18]*University of New Mexico, Albuquerque, New Mexico 87131*
[19]*Osaka City University, Osaka 588, Japan*
[20]*Universita di Padova, Istituto Nazionale di Fisica Nucleare, Sezione di Padova, I-35131 Padova, Italy*
[21]*University of Pennsylvania, Philadelphia, Pennsylvania 19104*
[22]*Istituto Nazionale di Fisica Nucleare, University and Scuola Normale Superiore of Pisa, I-56100 Pisa, Italy*
[23]*University of Pittsburgh, Pittsburgh, Pennsylvania 15260*
[24]*Purdue University, West Lafayette, Indiana 47907*
[25]*University of Rochester, Rochester, New York 14627*
[26]*Rockefeller University, New York, New York 10021*
[27]*Rutgers University, Piscataway, New Jersey 08854*
[28]*Academia Sinica, Taiwan 11529, Republic of China*
[29]*Superconducting Super Collider Laboratory, Dallas, Texas 75237*
[30]*Texas A&M University, College Station, Texas 77843*
[31]*Texas Tech University, Lubbock, Texas 79409*
[32]*University of Tsukuba, Tsukuba, Ibaraki 305, Japan*
[33]*Tufts University, Medford, Massachusetts 02155*
[34]*University of Wisconsin, Madison, Wisconsin 53706*
[35]*Yale University, New Haven, Connecticut 06511*
(Received 14 August 1997; published 19 December 1997)

We present the first measurement of the jet pseudorapidity distribution in direct photon events from a sample of $p\bar{p}$ collisions at $\sqrt{s}=1.8$ TeV, recorded with the Collider Detector at Fermilab. Quantum chromodynamics (QCD) predicts that these events are primarily from hard quark-gluon Compton scattering, $qg\rightarrow q\gamma$, with the final state quark producing the jet of hadrons. The jet pseudorapidity distribution in this model is sensitive to parton momentum fractions between 0.015 and 0.15. We find that the shape of the measured pseudorapidity distribution agrees well with next-to-leading order QCD calculations. [S0556-2821(98)01803-7]

PACS number(s): 13.85.Qk, 12.38.Qk

I. INTRODUCTION

Direct photon production in high energy hadron-hadron interactions provides a precise test of quantum chromodynamics (QCD), because photons produced in the primary interaction are not affected by subsequent strong interactions. Previous studies have traditionally measured the transverse momentum (P_T) [1] distribution of the photon. In this paper we examine the jet recoiling opposite the direct photon produced in $p\bar{p}$ collisions at $\sqrt{s}=1.8$ TeV, as recorded by the Collider Detector at Fermilab (CDF) [2]. Specifically, we present the first measurement of the shape of the jet pseudorapidity distribution, where the jet pseudorapidity, η_j, is $-\ln(\tan\theta_j/2)$, and θ_j is the polar angle of the jet relative to the proton beam. In this analysis the jet pseudorapidity distribution is the differential cross section, $d^3\sigma/d\eta_j d\eta_\gamma dP_T$, integrated over the photon transverse momentum interval of $16<P_T<40$ GeV/c, and a photon pseudorapidity (η_γ) interval of $|\eta_\gamma|<0.9$.

Photons directly produced in the initial interaction, in contrast with those from subsequent particle decays, are of interest because they provide a clean test of QCD and a constraint on the parton distribution functions for the proton. In leading order QCD, direct photons are produced by Compton scattering ($qg\rightarrow q\gamma$) and $q\bar{q}$-annihilation ($q\bar{q}\rightarrow g\gamma$), with Compton scattering contributing about 90% of the cross section in the kinematic range of this analysis. These production modes result in a jet of particles coming from the fragmentation of the recoiling parton. The cross sections for these processes have been calculated to next-to-leading order [3] (NLO) accuracy with QCD. Our measure-

*Visitor.

ment of the η_j distribution extends to ± 2.8, which, together with the aforementioned photon kinematic limits, defines the range of the parton momentum fractions (x) that are probed. The kinematic correspondence between jet pseudorapidity and parton x is illustrated in Fig. 1, where the high-x (x_H) and low-x (x_L) partons are shown as a function of jet pseudorapidity for the average photon P_T of this analysis [4]. The low-x parton momenta changes very little, while the high-x parton momenta ranges over $0.03<x<0.15$.

Previous measurements of the direct photon $d\sigma/dP_T$ distribution at $p\bar{p}$ colliders [5,6,7,8] have shown qualitative agreement with NLO QCD predictions over four orders of magnitude. However detailed comparisons have shown that the data have a somewhat steeper slope than QCD predicts for photons with $P_T<30$ GeV/c. The discrepancy in the P_T spectrum may be explained by the fact that the NLO QCD calculation only incorporates radiation from one additional initial state gluon, while nature can have photon production processes with multiple initial-state gluon emissions (extra ''K_T'') [9]. These extra gluon emissions can provide an additional transverse momentum boost to the photon-jet system, and therefore an additional smearing of the falling photon P_T spectrum. The smearing effect is largest for low P_T photons, and increases the observed cross section beyond that predicted by NLO QCD. However, since it has little effect at high P_T, it tends to make the P_T slope steeper in the data than in the calculation. In our measurement the average photon P_T is nearly the same for all jet pseudorapidities considered, and the K_T should therefore influence each η_j-bin nearly equally. Hence the shape of the η_j-distribution should be insensitive to this K_T effect and disagreements with NLO QCD due to this effect alone may not be apparent. However, if the deficit in the predicted number of photons at lower P_T can be accounted for by a modification in the gluon distribution of the proton [10], discrepancies may appear in the jet pseudorapidity distribution. We note that modification of the gluon distribution, although at higher x ($x>0.3$), has been proposed [11] to explain a discrepancy between data and NLO QCD calculations of the inclusive jet cross section measured by CDF and D0 [12,13].

II. CDF DETECTOR AND PHOTON IDENTIFICATION

The data presented here correspond to an integrated luminosity of 16 pb^{-1} of $p\bar{p}$ collisions collected by CDF in the 1992–1993 Tevatron collider run, and is the same data sample used in a previously published direct photon P_T measurement [6]. The primary components of the detector relevant for this analysis are those that determined the $p\bar{p}$ collision vertex, and measured photon and jet kinematics: the vertex tracking chamber, the central tracking chamber (CTC), and the calorimeters. The $p\bar{p}$ vertex defines the origin of the coordinate system [1] used to determine the polar angle, θ, of the photon and jet. The CTC is used to detect charged particles. The electromagnetic (EM) and hadronic calorimeters are used for jet identification. The calorimeters, which extend out $\eta=\pm 4.2$, have a projective $\eta-\phi$ tower geometry [14]. The tower segmentation is $\Delta\eta\times\Delta\phi\approx 0.1\times 15°$ for the EM (hadronic) calorimeter out to pseudorapidities of ± 1.1 (± 1.3), and $\approx 0.1\times 5°$ for higher pseudorapidities. Jets are identified from their clustering of transverse energy, E_T, in the $\eta-\phi$ grid of the calorimeter towers. The standard CDF jet clustering algorithm [15] is used with a jet cone radius of 0.7, where the radius is the distance from the cluster centroid, $\Delta R=\sqrt{\Delta\eta^2+\Delta\phi^2}$. Photon candidates are required to be within the central region ($|\eta|<1.1$) of the EM calorimeter where improved photon discrimination against background is possible due to the presence of the central preshower (CPR) chambers and the central electromagnetic strip (CES) chambers. The CPR chambers are located in front of the EM calorimeter and they sample electromagnetic showers that begin in the 1.08 radiation length thick solenoidal magnet coil directly in front of them. The CES chambers, embedded in the EM calorimeter near shower maximum, are used to measure the transverse profiles of showers.

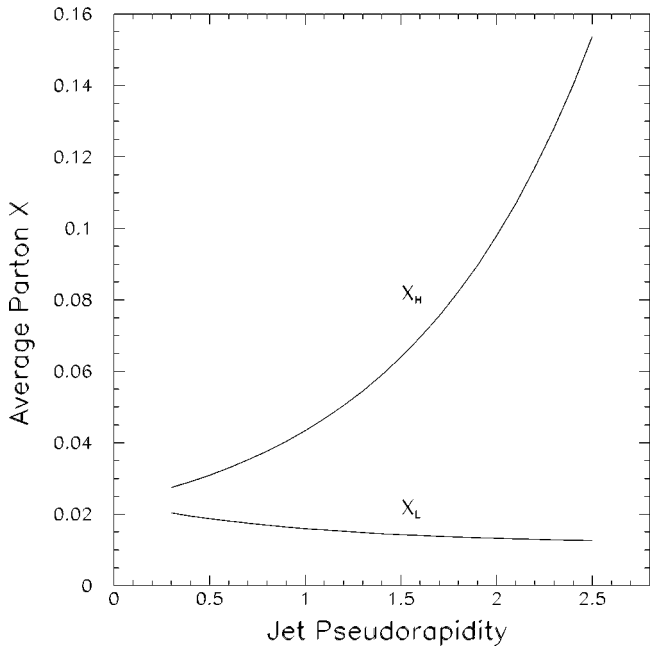

FIG. 1. The momentum fractions of the high (x_H) and low (x_L) x partons required to produce a jet at the specified $|\eta_j|$ recoiling against a photon of $P_T=21$ GeV/c and $\eta_\gamma=0$, the mean values for this analysis.

The events used in this analysis contain an isolated cluster of energy in the central EM (CEM) calorimeter with no charged tracks pointing to the cluster. These events are selected by a trigger that requires a photon candidate to be above a P_T threshold of 16 GeV/c and to be isolated, with $E_{iso}(0.7)<2$ GeV. Here, $E_{iso}(0.7)$ is the transverse energy in a cone of $\Delta R<0.7$ around the candidate, but excluding the energy of the candidate. Photon candidates are required to pass the fiducial and selection cuts summarized in references [5,6]. A requirement of no more than one energy cluster per CES chamber reduces the background from photons from $\pi^0\rightarrow\gamma\gamma$ and $\eta\rightarrow\gamma\gamma$ decays. About half of the photon candidates that pass the cuts are from these decays where both photons overlap in the CES, and are not readily distinguishable from single photons on an event-by-event basis. They are distinguishable on a statistical basis by using the background subtraction methods described in references [5,6]. The systematic uncertainty on an absolute cross section measurement from the background subtraction is 8%, but in this analysis (which is the ratio of cross sections at different jet

TABLE I. The fraction of events with multiple jets as function of the minimum jet E_T.

Minimum E_T (GeV)	Fraction of Events
5	82.8%
10	40.5%
15	12.4%

pseudorapidities) the uncertainty is reduced to less than 1% and is negligible.

III. JET INFORMATION AND CORRECTIONS

After the photon backgrounds are subtracted, the jet information in the events must be corrected to match the NLO QCD calculations to which the measurements will be compared. The calculations include the $2\rightarrow 2$ processes, $qg\rightarrow\gamma q$ and $q\bar{q}\rightarrow g\gamma$, as well as the higher order virtual corrections to these processes. In addition, the calculations include at tree-level $2\rightarrow 3$ processes that contain an energetic second jet, but these terms have larger theoretical uncertainties. Thus one would like to limit the number of events with an energetic second jet. Another reason to reduce such a process is that the available calculations are at the parton level, and are without fragmentation effects or an underlying event from spectator interactions which may also produce an energetic second jet. In this analysis all jets identified by the standard CDF jet clustering algorithm are considered as candidates to be the jet arising from the $2\rightarrow 2$ process. The fraction of events with multiple jets is large, as is shown in Table I. The data's $\Delta\phi_{\gamma j}$ distribution for the largest E_T jet is shown in Fig. 2, where $\Delta\phi_{\gamma j}$ is the difference in the jet and photon azimuthal angles. Events with the $2\rightarrow 2$ topology occupy the peak at 180°. The width of the distribution due to detector effects alone is expected to be $\approx 3°$, but the data are much broader than this, indicating that the physics effects discussed above appear to be significant. Thus, events in the shoulders of the distribution generally have an energetic second jet in the event. To illustrate this the ratio of second-largest jet E_T to largest jet E_T is shown in Fig. 3. This figure shows the E_T ratio for all events with a second jet, and also with an additional cut $150°<\Delta\phi_{\gamma j}<210°$. One can see that there is a correlation between the difference in azimuthal angles between the jet and photon, and the presence of an energetic second jet. Therefore we will use the $\Delta\phi_{\gamma j}$ restriction to improve the selection of data satisfying the $2\rightarrow 2$ scattering topology. The $\Delta\phi_{\gamma j}$ cut is a kinematic limit. This limit, and the others used for the jet pseudorapidity measurement are summarized in Table II.

The jet pseudorapidity distribution is symmetric about $\eta_j=0$ at the Tevatron collider, so the data are partitioned into pseudorapidity bins of $|\eta_j|$. In order to compare these data with NLO QCD calculations, one must apply various corrections to the data. The data are corrected for photon acceptance within $|\eta_\gamma|<0.9$, which includes the trigger and selection efficiencies and is $\approx 39\%$ on average. In addition, the data's jet pseudorapidity distribution must also be corrected. Even with the $\Delta\phi_{\gamma j}$ cut described above, the effets of parton fragmentation, detector response, and jet reconstruction can lead to events where the reconstructed jet is in a different η bin than the original parton. It is also possible due to detector resolution for a second jet in the event to be misidentified as the primary jet, and this second jet could be in a different η bin than the primary parton. In addition, a small ($<1\%$) fraction of events do not have a reconstructed jet. Therefore we have used a QCD Monte Carlo program and a detector simulation to correct the jet distribution back to the parton level, and we call this correction the parton acceptance, P_{acc}. The parton acceptance is calculated using the leading order PAPAGENO [16,17] Monte Carlo program that generates $qg\rightarrow q\gamma$ and $q\bar{q}\rightarrow g\gamma$ interactions. The interaction is given a transverse momentum boost (K_T) to simulate the effects of all gluon radiation. This K_T boost is tuned on CDF dijet data [15], and the same boost is observed to bring the simulated $\Delta\phi_{\gamma j}$ distribution into agreement with the data. The outgoing partons are fragmented into jets of particles, with an empirical fragmentation model based on CDF data [15]. Underlying event energy is added using a model also tuned on CDF dijet data. Finally, the detector response is simulated and the results are analyzed as data. The detector resolution effects are determined using jets up to an η_j of ± 4.2. Such large pseudorapidities are important in order to constrain the corrections for smearing across η_j-bins as the resolution worsens for increasing η_j. Table III gives the range of each pseudorapidity bin, the parton acceptance, and the corrected number of events. The corrections to the number of events include both the photon and parton acceptance. Also tabulated is the fully-corrected $|\eta_j|$ distribution, $R(\eta_j)$, which is the corrected event distribution normalized to 1.0 in the $0<|\eta_j|<0.7$ bin. The quantity $R(\eta_j)$ is just the ratio of cross sections integrated over the kinematic limits specified in Table II: $d\sigma/d\eta_j$ normalized to

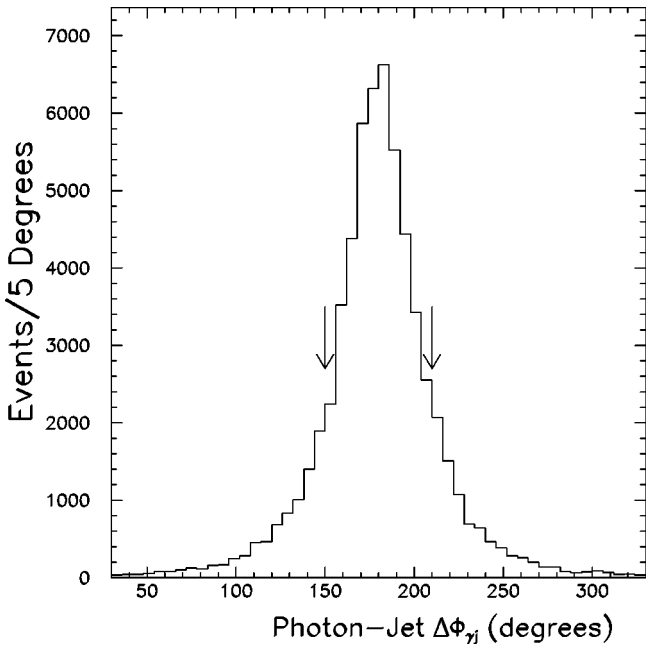

FIG. 2. The difference in azimuthal angle, $\Delta\phi_{\gamma j}$, between the photon and the highest E_T jet is shown for the data. The arrows give the outer limits of the back-to-back restriction used in this analysis.

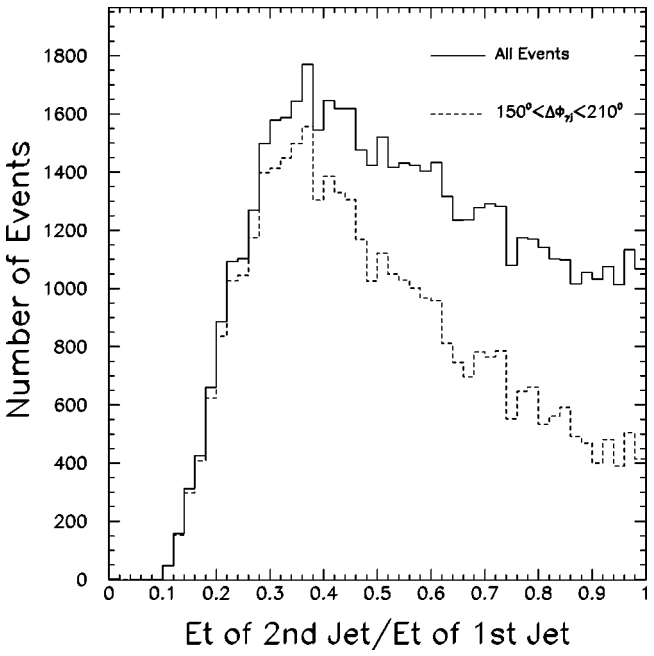

FIG. 3. The ratio of jet E_T for the second largest E_T jet and the largest E_T jet is shown, if a second jet is present. The dashed line is with the photon-jet $\Delta\phi_{\gamma j}$ cut as discussed in the text.

$d\sigma/d\eta_j$ $(0<|\eta_j|<0.7)$. The measured values are shown in Fig. 4, with statistical uncertainties only.

IV. SYSTEMATIC UNCERTAINTIES

The measurement of $R(\eta_j)$ has eight different sources of systematic uncertainty [18], listed in Table IV. The systematic uncertainties listed in Table III are the quadrature sum of the uncertainties given in Table IV. The first uncertainty due to the photon background subtraction was discussed earlier and is less than 1%. The second systematic uncertainty is due to the detector simulation of the CDF calorimeters in the regions between detector boundaries. The CDF calorimetry is not hermetic and in the noninstrumented regions the energy response for a jet is affected. This can change the reconstructed pseudorapidity of the jet and therefore the parton acceptance P_{acc}. The uncertainty is obtained by varying the calorimetry response in the boundary towers from no energy to 50% more than nominal. This may appear an extreme variation, but since the boundary towers subtend a small fraction of the complete jet, this variation is on average a few percent variation of the jet energy, which is consistent with the jet energy uncertainties determined with constraints from the transverse momentum balance with the photon. This is

TABLE II. The kinematic limits of the jet pseudorapidity measurement. The photon pseudorapidity and transverse momentum are given by η_γ and P_T respectively. The difference between photon and jet azimuthal angles is given by $\Delta\phi_{\gamma j}$.

$\lvert\eta_\gamma\rvert<0.9$
$16<P_T<40$ GeV/c
$150°<\Delta\phi_{\gamma j}<210°$

TABLE III. The parton acceptance, P_{acc}, and the number of events (N_{ev}) per bin corrected for the photon trigger, selection efficiencies, and the parton acceptance. The fully-corrected jet pseudorapidity distribution, $R(\eta_j)$, is normalized so that $R(\eta_j)\equiv 1.00$ in the first η bin. The ''Stat.'' and ''Sys.'' uncertainties are the percentage statistical and systematic uncertainties on N_{ev} and $R(\eta_j)$.

$\lvert\eta_j\rvert$ Bin: Range	P_{acc}	N_{ev}	$R(\eta_j)$ data	Stat. Error(%)	Sys. Error(%)
1: 0.0–0.7	0.953	49266	$\equiv 1.000$	-	-
2: 0.7–1.4	0.976	37894	0.769	2.8	5.8
3: 1.4–2.1	0.918	24012	0.487	3.9	10.3
4: 2.1–2.8	1.20	13270	0.269	7.2	14.8

the largest uncertainty in the analysis, an 8% uncertainty in the highest two η_j bins. The third systematic uncertainty explores the sensitivity of the analysis to the $\Delta\phi_{\gamma j}$ limit. The limit is varied by $\pm 10°$ and the entire analysis repeated, giving rise to 3% changes in $R(\eta_j)$. The fourth uncertainty is due to the slight sensitivity of the parton acceptance corrections to changes in the shape of the simulated η_j spectrum. Since the main theoretical variation in this shape is due to the input parton distribution functions, we take the difference in P_{acc} when changing the parton distributions from the default [17] to CTEQ2ML as the uncertainty (changing to CTEQ2MF gave the same variation).

The remaining four systematic uncertainties are due to the event generation used in constructing the parton acceptance corrections P_{acc}. These are uncertainties in the comparison of data and NLO QCD, rather than in the measurement itself. Any uncertainties in the basic comparison of data and NLO QCD must be examined, and we include them in the ''experimental'' uncertainties in this paper. A complete QCD model would include the four effects we are concerned with:

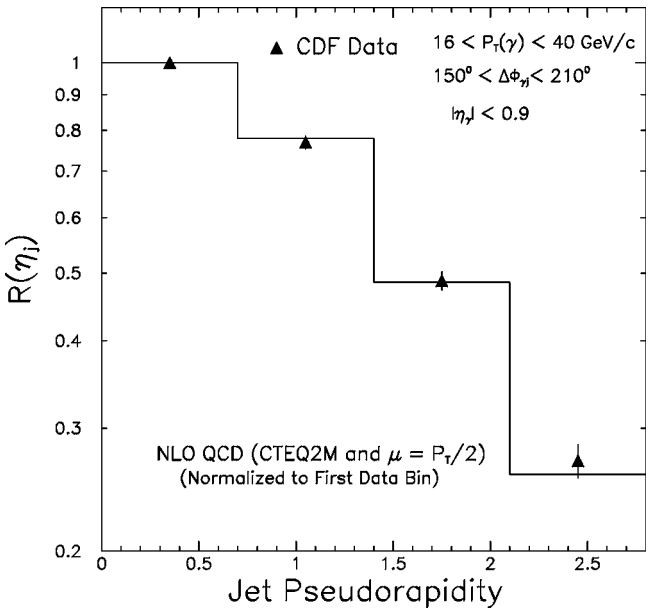

FIG. 4. The fully-corrected shape of the $|\eta_j|$ distribution, $R(\eta_j)$, is shown for the data with statistical uncertainties only. A NLO QCD calculation is also shown for comparison (see text).

TABLE IV. The systematic errors associated with various aspects of the measurement of the parton pseudorapidity distribution. The last four entries are uncertainties in the comparison of data with the NLO QCD model, rather than the measurement itself.

Source of uncertainty	$\|\eta_j\|$ bin 0.0–0.7	$\|\eta_j\|$ bin 0.7–1.4	$\|\eta_j\|$ bin 1.4–2.1	$\|\eta_j\|$ bin 2.1–2.8
Multiphoton background subtraction	-	<1%	<1%	<1%
Detector simulation	-	5%	8%	8%
$\Delta\phi_{\gamma j}$ limit variation	-	3%	3%	3%
Slope of η_j distribution	-	<1%	<1%	2%
Parton fragmentation	-	2%	3%	7%
Initial state parton shower	-	1%	3%	8%
Underlying event	-	<1%	5%	3%
Higher order QCD	-	1%	1%	2%

(1) the fragmentation of the final state partons into jets, (2) full initial state parton showers (K_T), (3) an underlying event from spectator interactions, and (4) higher order QCD effects that give rise to an energetic second jet. These four effects are highly correlated with each other. There is no way to separate them in the data or in a complete QCD model, but our event generator introduces these effects empirically and we are able to vary them individually to estimate the systematic uncertainty for each [18]. For example, the higher order QCD uncertainty is obtained by varying the mixture of leading order $2\rightarrow2$ events and higher order $2\rightarrow3$ events. The resulting change in the measurement is shown in Table IV, as well as the uncertainties obtained by varying the parton fragmentation, underlying event, and K_T used in the event generator.

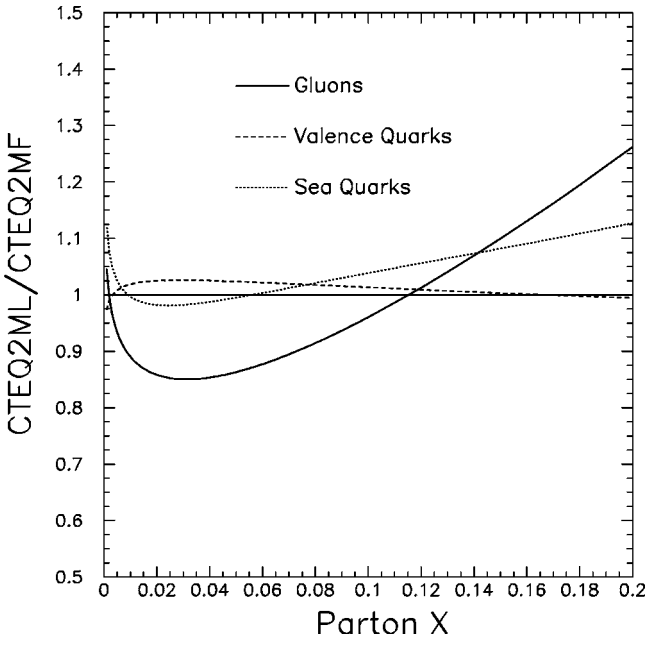

FIG. 5. The CTEQ2ML and CTEQ2MF parton distribution sets are compared in the x and Q^2 range relevant for this measurement. The main difference between these two sets is in the shape of the gluon distribution.

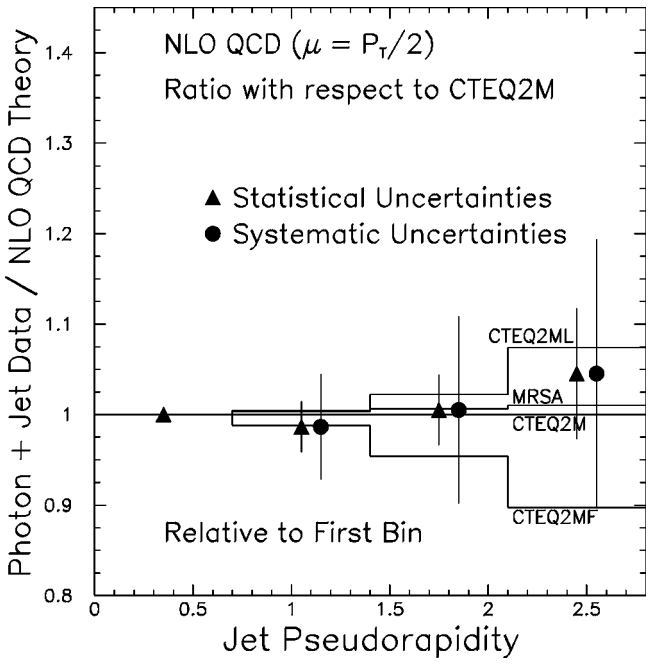

FIG. 6. A shape comparison between the $|\eta_j|$ distribution in the data and the NLO QCD calculation on a linear scale. The data are divided by the NLO QCD calculation with CTEQ2M parton distributions, and normalized to unity in the first bin.

V. COMPARISON WITH NLO QCD

The normalized pseudorapidity distribution, $R(\eta_j)$, is plotted in Fig. 4 along with a NLO QCD calculation [3] of the cross section ratio. The calculation uses a typical factorization and renormalization scale used in direct photon calculations, $\mu = P_T/2$, and the CTEQ2M [19] proton parton distribution functions. There is good agreement between the measurement and the calculation. The same conclusion is reached if comparing to the most recent parton distributions from CTEQ, namely CTEQ4M [20]. The NLO QCD calculation using CTEQ4M is only a few % below CTEQ2M in the last η_j bin.

A more detailed comparison of the measured η_j distribution with QCD may be made by considering different scales and parton parameterizations. Since the inclusive photon cross section measurement from CDF [6] compared to the CTEQ2M parton distributions, we will use these parton sets to compare to as well. The contrast between different parton distributions may be clarified by the following considerations. For this analysis the average momentum fractions of the initial state partons probe the range from $x = 0.015$ to 0.15, as discussed earlier and shown in Fig. 1. The variations [19,21] among sets of parton distributions in this x-range are due primarily to the differing gluon and sea quark distributions. Figure 5 shows how CTEQ2ML and CTEQ2MF differ in the behavior of the gluons whereas the valence quarks show only a small variation over the x-range of this analysis. Furthermore, since the sea quarks are derived from the gluons, even the small changes there are driven primarily by changes in the gluons. Hence, this measurement is primarily sensitive to changes in the slope of the gluon distribution from $x = 0.015$ to 0.15.

To make differences between the data and the theory more discernable, Fig. 6 shows the data divided by the NLO QCD calculation with CTEQ2M parton distributions, and normalized to unity in the first bin. The NLO QCD calculations using various other parton distributions are subjected to the same procedure and are also presented in the same figure for comparison. The Martin-Roberts-Stirling set A (MRSA) [21] parton distributions are a ''best-fit'' parameterization similar to the CTEQ2M distributions. The lower theory curve, such as CTEQ2MF, are those where the gluon parameterizations fall more rapidly with increasing x in our kinematic range. The systematic uncertainties are also shown in Fig. 6. The deviations between data and theory were tested using a standard covariance-matrix χ^2 test, which included the bin-to-bin jet pseudorapidity correlations of the various components of the systematic error. We find all of the parton parameterizations in Fig. 6 are consistent with data within one standard deviation. Changing the renormalization scale to $\mu = P_T$ moves all the theoretical curves down by 7% at the largest η_j in Fig. 6, but does not change the basic conclusions drawn with the scale $\mu = P_T/2$. The sets of parton distributions tested are only meant to be a representative sample. Parameterizations with gluon distributions that fall more rapidly than CTEQ2MF may still be allowed by other measurements used in the standard global QCD analyses [19,21], yet would be disfavored by this measurement. Therefore these data could provide an important constraint once incorporated into the global analyses of parton distribution functions.

VI. SUMMARY

We have presented the first measurement of the jet pseudorapidity distribution in direct photon events in $p\bar{p}$ collisions at $\sqrt{s} = 1.8$ TeV. The shape of the jet pseudorapidity distribution agrees well with NLO QCD calculations, even though previous photon P_T measurements have shown an excess at low P_T. This may be due to the insensitivity of this measurement to multigluon emissions, which is one explanation of the low P_T excess. This analysis is unable to discriminate clearly between the four parton parameterizations tested. Nevertheless, the present data provide a new type of constraint on the shape of the gluon distribution in global QCD analyses. Our analysis also lays the groundwork for future measurements of jet pseudorapidity with higher P_T photons. Such data would probe increasing x-values, perhaps extending above 0.3 where large changes in the gluon distribution have recently been proposed to explain the inclusive jet cross section from CDF and D0.

ACKNOWLEDGMENTS

We thank the Fermilab staff and the technical staffs of the participating institutions for their vital contributions. This work was supported by the U.S. Department of Energy and National Science Foundation; the Italian Istituto Nazionale di Fisica Nucleare; the Ministry of Education, Science and Culture of Japan; the Natural Sciences and Engineering Research Council of Canada; the National Science Council of the Republic of China; the A. P. Sloan Foundation; and the Swiss National Science Foundation.

[1] The coordinate system used is (θ,ϕ), where θ is the polar angle relative to the proton beam as measured from the event vertex, and ϕ the azimuth. The photon transverse momentum is $P_T = \mathrm{P}\sin(\theta)$, where P is the photon momentum.

[2] F. Abe *et al.*, Nucl. Instrum. Methods Phys. Res. A **271**, 387 (1988), and the references therein.

[3] J. Ohnemus, H. Baer, and J. F. Owens, Phys. Rev. D **42**, 61 (1990).

[4] The momentum fractions of the two initial state partons, x_H and x_L, are calculated using, $x_{H,L} = (P_T/c\sqrt{s})(e^{\pm\eta_\gamma} + e^{\pm\eta_j})$. Here, $x_H > x_L$, and the momentum fractions are in the $p\bar{p}$ center-of-momentum frame, P_T is the average photon transverse momentum in this analysis, and $\sqrt{s}$ is the $p\bar{p}$ center-of-momentum energy.

[5] CDF Collaboration, F. Abe *et al.*, Phys. Rev. Lett. **68**, 2734 (1992); Phys. Rev. D **48**, 2998 (1993).

[6] CDF Collaboration, F. Abe *et al.*, Phys. Rev. Lett. **73**, 2662 (1994).

[7] D0 Collaboration, S. Abachi *et al.*, Phys. Rev. Lett. **77**, 5011 (1996).

[8] UA2 Collaboration, J. Alitti *et al.*, Phys. Lett. B **263**, 544 (1991).

[9] H. Baer and M. H. Reno, Phys. Rev. D **54**, 2017 (1996); J. Huston *et al.*, *ibid.* **51**, 6139 (1995).

[10] W. Vogelsang *et al.*, Nucl. Phys. **B453**, 334 (1995).

[11] H. L. Lai *et al.*, Phys. Rev. D **55**, 1280 (1997).

[12] CDF Collaboration, F. Abe *et al.*, Phys. Rev. Lett. **77**, 438 (1996).

[13] D0 Collaboration, S. Abachi *et al.*, Fermilab-CONF-96/304-E (1996).

[14] For calorimetry, the pseudorapidity, $\eta = -\ln\tan(\theta/2)$, is used to define the location of a calorimeter tower. The transverse energy, E_T in a tower is $E\sin\theta$, where E is the energy deposited in the tower.

[15] CDF Collaboration, F. Abe *et al.*, Phys. Rev. D **45**, 1448 (1992).

[16] I. Hinchliffe, in *Proceedings of the Workshop on Physics at Current Accelerators and the Supercollider*, Argonne, Illinois, 1993, edited by J. L. Hewett *et al.* (ANL Report No. 93-92, Argonne, 1993).

[17] M. Diemoz, F. Ferroni, E. Longo, and G. Martinelli, Z. Phys. C **39**, 21 (1988).

[18] C. Hawk, Ph.D. thesis, Rutgers University, 1996.

[19] H. L. Lai *et al.*, Phys. Rev. D **51**, 4763 (1995).

[20] H. L. Lai *et al.*, Phys. Rev. D **55**, 1280 (1997).

[21] A. D. Martin, W. J. Stirling, and R. G. Roberts, Phys. Rev. D **50**, 6734 (1994).